NANO LETTERS

pubs.acs.org/NanoLett Letter

Spacer Matters: All-Peptide-Based Ligand for Promoting Interfacial Proteolysis and Plasmonic Coupling

Zhicheng Jin, Chuxuan Ling, Yi Li, Jiajing Zhou, Ke Li, Wonjun Yim, Justin Yeung, Yu-Ci Chang, Tengyu He, Yong Cheng, Pavla Fajtová, Maurice Retout, Anthony J O'Donoghue, and Jesse V. Jokerst*

Cite This: *Nano Lett.* 2022, 22, 8932–8940 Read Online

ACCESS | Metrics & More | Article Recommendations | Supporting Information

ABSTRACT: Plasmonic coupling *via* nanoparticle assembly is a popular signal-generation method in bioanalytical sensors. Here, we customized an all-peptide-based ligand that carries an anchoring group, polyproline spacer, biomolecular recognition, and zwitterionic domains for functionalizing gold nanoparticles (AuNPs) as a colorimetric enzyme sensor. Our results underscore the importance of the polyproline module, which enables the SARS-CoV-2 main protease (M^{pro}) to recognize the peptidic ligand on nanosurfaces for subsequent plasmonic coupling *via* Coulombic interactions. AuNP aggregation is favored by the lowered surface potential due to enzymatic unveiling of the zwitterionic module. Therefore, this system provides a naked-eye measure for M^{pro}. No proteolysis occurs on AuNPs modified with a control ligand lacking a spacer domain. Overall, this all-peptide-based ligand does not require complex molecular conjugations and hence offers a simple and promising route for plasmonic sensing other proteases.

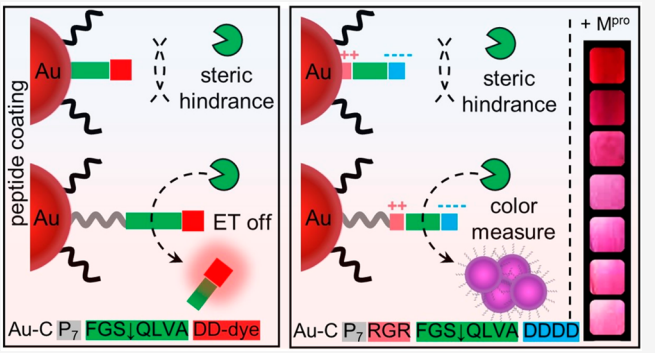

KEYWORDS: *SARS-CoV-2 M^{pro}, polyproline, interfacial proteolysis, plasmonic coupling, NEST, colorimetric sensor*

Molecular self-assembly can transduce and amplify biochemical analytes into physiochemical signals.[1−6] The assembly of ligand-protected inorganic nanoparticles (NPs) is particularly attractive because their optical properties change as a function of interparticle spacing. For instance, the coupled metallic NPs in close proximity leads to a collective plasmon and red-shifts the resonant wavelength relative to individual nanoparticles—this in turn causes color change.[7] In addition, coating molecules can cause NPs to respond to biomolecular stimuli *via* changes in affinity,[8−11] hydrophilicity,[12−14] charge valence,[15−19] or reactivity,[1,20] which subsequently induce colloidal aggregation and color changes suitable for sensing applications. Previous studies have provided some insights to guide the rationale design of coating ligand for better bionanoscale recognition, revealing that the collective architecture presented on nanosurfaces determines the accessibility, homogeneity, orientation, and functionality, *etc.*[21,22]

Assembly of NPs into larger structures has been reported by employing several types of biomolecules (*e.g.*, oligonucleotides,[23,24] enzymes,[25] peptides[26]). NP dimensions are comparable to those of many macromolecules, and thus a spacer module in coating ligand is the key to overcome steric repulsion between the nanosurfaces and targeting analytes and ensure molecular interactions.[27,28] For instance, synthetic alkane chains (*e.g.*, C_6) have been inserted into the antisense oligonucleotides for capping gold nanoparticles (AuNPs), which enables naked-eye diagnosis of SARS-CoV-2.[29] Likewise, molecular modeling and experimental results showed that the same alkyl block relieves kinase from steric hindrance in catalyzing the surface-bound substrates.[30] Alternatively, these synthetic linkers can be replaced with a natural oligonucleotide (*e.g.*, repeating thymine) for surface functionalization to form an all-DNA-based layer that directs AuNP-superlattice formation.[31] In other cases, proteases and their peptide substrates can organize nanostructures for colorimetric measure.[8]

In one example from our lab, we used a protease-activatable zwitterionic peptide with switchable electrophoretic properties—the peptide assembles the charged AuNPs following cleavage by SARS-CoV-2 main protease (M^{pro}).[16] Although effective at measuring proteases, this approach and others adapt a stepwise strategy: (*i*) incubation of enzyme with substrate and (*ii*) NP introduction.[10,17,32,33] This complicates the instructed processes for end-users from using the point-of-

Received: August 2, 2022
Revised: October 30, 2022
Published: November 8, 2022

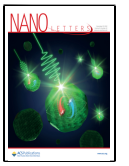

https://doi.org/10.1021/acs.nanolett.2c03052
Nano Lett. 2022, 22, 8932−8940

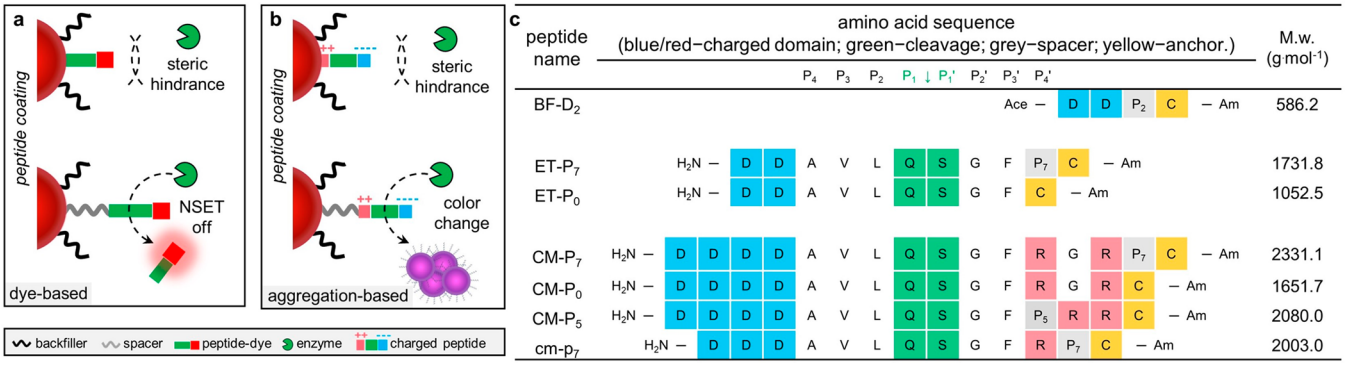

Figure 1. Modular peptide design for energy transfer (ET) and colorimetric (CM) sensing of SARS-CoV-2 M^{pro}. A spacer domain is required to reduce steric hindrance and allows for proteolytic activation of optical signals in (a) nanosurface energy transfer (NSET) sensors adopting a sandwiched AuNP−peptide−dye and in (b) colorimetric sensors using zwitterionic peptide-coated AuNPs. (c) Thiolate peptide ligands include the backfiller (BF-D_2), M^{pro} substrates for NSET (ET-P_7 and ET-P_0) and colorimetric (CM-P_7 and CM-P_0) model. *Remark:* CM-P_5 peptide switches the polyPro scaffold and Arg domain, and cm-p_7 contains only one Arg. Amino acids on the critical modules are color coded; *i.e.*, M^{pro} cleaves at Q↓S (P1 and P1′ site).

care diagnostic kit. Strategies that render proteolysis and plasmonic coupling in one pot have mainly focused on conjugating substrates onto polymeric ligands such as poly(ethylene glycol) (PEG) and extending the spatial distance for biointeractions.[18,20,28,34] Nonetheless, the PEGylation process, conjugate purification, and postreaction evaluation remain complex. Furthermore, PEG could make NP-based colorimetric sensors challenging due to the great steric stabilization offered by the entropy-driven polymeric architecture, thus impeding NP coagulation.[35] In comparison, the polyproline (polyPro, or P_x) helix is a neutral, compact, and rigid linker with simultaneous good water-solubility and hydrophobicity due to the lack of intramolecular hydrogen bonds.[36−38] The favorable hydrophobic interactions among polyPro segments patterned tight self-assembled monolayers on nanosurfaces.[39,40] This motivated us to explore a polyPro as an alternative spacer in a ligand for coating NPs and directing *in situ* plasmonic coupling.

We validated this NP−peptide construct for detecting the SARS-CoV-2 M^{pro} through two models including an energy transfer (ET)-based AuNP−peptide−dye and a color-based AuNP−zwitterion−peptide conjugate. The peptide consisted of a surface anchoring group, a neutral spacer, a biomolecular recognition element, and a zwitterionic domain. M^{pro} was selected as the target enzyme due to its important function in protein postprocessing of the SARS-CoV-2 polypeptide.[41] We hypothesized that inclusion of polyPro in the ligand would promote interfacial proteolysis and ensure a compact coating for plasmonic coupling (*i.e.*, length of $P_7 \approx 2.1$ nm;[42,43] the size of monomeric M^{pro} at 33 kDa is about 2−4 nm[41,44]). The role of spacer was first validated in a typical ET-based configuration (*i.e.*, AuNP−peptide−dye, Figure 1a) where the polyPro module enabled M^{pro}-activatable photoluminescence (PL) recovery and *vice versa*. We then compared the M^{pro}-mediated aggregation of AuNPs modified with the zwitterionic ligand (*i.e.*, CM-P_7 sequence: D_4AVLQ↓SGFRGRP_7C, Figure 1b) versus a control ligand (*i.e.*, CM-P_0: D_4AVLQ↓SGFRGRC, no P_7). Here, the polyPro linker also allowed successful interfacial proteolysis, which lowered the surface potential to an unstable regime (*e.g.*, −10 to 0 mV), thus providing a color readout of M^{pro} with a detection limit of 50 nM.

Validation in NSET Model. The interactions of plasmonic surfaces with proximal dye emitters result in efficient PL quenching.[45] This has been referred to as nanosurface energy transfer (NSET), a popular strategy of signal transduction for developing analytical biosensors.[46] Figure 1a illustrates the configuration of NSET-based enzymatic sensors involving a peptide linker, *i.e.*, AuNP−peptide−dye conjugate (13 nm AuNP by Turkevich method[47]). Here we embedded two peptides in the conjugates for M^{pro} detection: D_2AVLQ↓SGFP_7C (named ET-P_7) and D_2AVLQ↓SGFC (ET-P_0, control) (Figure 1c). The ET-P_7 peptide was rationally designed to encompass five functional domains including (*i*) a terminal amino for *N*-hydroxysuccinimide (NHS)-dye labeling, (*ii*) dihomo Asp (D_2) for promoting NP stabilization, (*iii*) an M^{pro} recognition site, (*iv*) a polyPro spacer, and (*v*) a Cys anchor. The negative control (ET-P_0) lacked the P_7 domain. Proteolysis of the peptide by M^{pro} was confirmed by ESI-MS (Figure S1). Indeed, cleavage at the C-terminal side of Gln (Q) is rarely seen for human proteases except for kallikrein-3 that is expressed only in the prostate.[48] We note that a short and acetylated peptide in the DDPPC sequence (Figure 1c) was used as a backfiller (or inert ligand) with the above peptides to control the surface density of the M^{pro} substrate.

We selected NHS-TAMRA dye as NSET-donor because it has a sizable spectral overlap with AuNP absorption (Figure 2a). Successful peptide-TAMRA conjugation (*i.e.*, ET-P_7T and ET-P_0T) *via* NHS-amine chemistry was confirmed by MALDI-TOF MS (Figure S1). AuNP−peptide−dye conjugates were then prepared by ligating citrate−AuNPs with ET-P_7T and BF-D_2 at a molar ratio of 20:80.[49] Purification was performed using size exclusion chromatography (*i.e.*, PD-10 column with Sephadex G25):[45,50] The first eluted band containing Au conjugates had remarkable separation from the second band of unbound ET-P_7T and was collected for further use (Figure 2b). Figure 2c shows the absorbance of polyvalent AuNP−(ET-P_7T)$_n$ conjugates and deconvoluted contribution from AuNP and dye component. The valence number, $n = 257$, is extracted by comparing the deconvoluted absorbance to their molar absorption coefficients, *i.e.*, $\varepsilon_{520\ nm} = 6.58 \times 10^7\ M^{-1}\ cm^{-1}$ for AuNP and $\varepsilon_{554\ nm} = 8.0 \times 10^4\ M^{-1}\ cm^{-1}$ for TAMRA.[51] Figure 2d shows a substantial loss (96.8%) in the dye PL after AuNP conjugation. A weak collisional quenching of 41.3% was measured from a mixture of AuNPs and free ET-

https://doi.org/10.1021/acs.nanolett.2c03052
Nano Lett. 2022, 22, 8932−8940

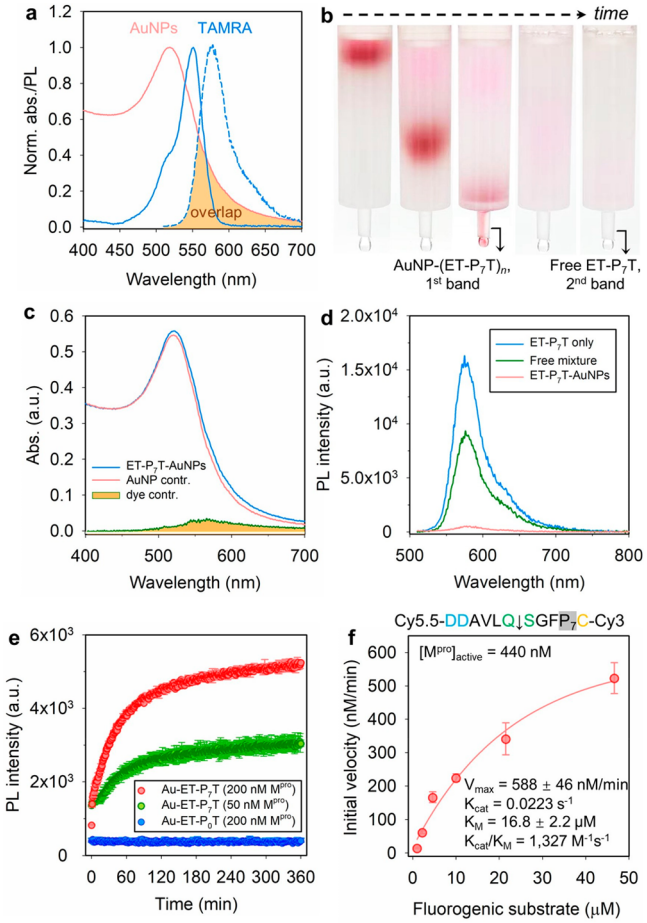

Figure 2. Inclusion of polyPro enables NSET-sensor activation by M^{pro}. (a) Normalized optical spectra of AuNP and TAMRA dye, along with their spectral overlap. Abs. = full lines, and photoluminescence (PL) = dash line. (b) Time-lapsed images of size exclusion chromatography for purifying AuNP conjugates (1st band, retention time = 1 min) from the free peptide–dye (2nd band, retention time = 10 min). (c) Abs. spectral deconvolution of the AuNP–$(ET\text{-}P_7T)_n$ conjugates yields AuNP and dye contribution; valence number, n = 257. (d) PL spectra collected from free ET-P_7T, AuNPs mixed with ET-P_7T, and AuNP–$(ET\text{-}P_7T)_n$ conjugates. (e) Time-dependent $PL_{580\ nm}$ changes of AuNP–$(ET\text{-}P_7T)_{257}$ and AuNP–$(ET\text{-}P_0T)_{241}$ conjugates incubated with M^{pro} (50 or 200 nM). Error bars = standard deviations (duplicates). (f) k_{cat}/K_M determination for hydrolysis of the ET-P_7 by M^{pro} in 10 mM PB, pH 8.0, at 37 °C. The M^{pro} (440 nM, by titration) was incubated with the fluorogenic substrate ($[S]_0$ = 0–50 μM, sequence shown on top), and the product concentration at 30 min was determined. Data were fitted to the Michaelis–Menten equation (eq S13).

P_7T (control); see more NEST analysis in Supporting Information.

The AuNP–$(ET\text{-}P_7T)_{257}$ and AuNP–$(ET\text{-}P_0T)_{241}$ conjugates were incubated with M^{pro}, and their kinetics were compared. Figure 2e shows a clear enhancement in the dye PL for AuNP–$(ET\text{-}P_7T)_{257}$ with up to 10-fold recovery at 6 h. This indicates that approximately 60% of the docked ET-P_7T substrate were liberated from nanosurfaces, assuming that the PL intensity for a mixed AuNPs/ET-P_7T corresponds a full digestion. On the contrary, AuNP–$(ET\text{-}P_0T)_{241}$ showed no signal activation. This discrepancy in the PL kinetics validated the key role of P_7 spacer in the peptide design, which allows for successful interfacial proteolysis and turn-on of PL signals in a NSET model.

The kinetics of signal activation were relatively long (Figure 2e). To understand the reason, we determined the specificity constant (k_{cat}/K_M) for ET-P_7 by M^{pro} using a fluorogenic substrate (Cy3-ET-P_7–Cy5.5; Figure S4) and was 1,327 M^{-1} s^{-1}, which is 2.5-fold less than that from a previous work,[52] presumably because of the alternation of P4′ residues from Arg to Pro.[53] Thus, the slow detection seen here is a function of the *protease* and not a function of the *detection* system. Detailed kinetic analysis was provided in the Supporting Information. In addition, this fluorogenic substrate enabled Förster resonance energy transfer (FRET), a spectroscopic ruler, to measure the impact of sterics.[54] The overlap integral for Cy3-Cy5.5 pair is 3.4×10^{-13} M^{-1} cm^3,[35] and the Förster distance (R_0) is 3.7 nm. The measured FRET quenching efficiency was 82.8% for Cy3-ET-P_7–Cy5.5 (Figure S4f). Thus, the estimated donor–acceptor distance was 2.9 nm (eq S10), comprising of a P_7 block (2.1 nm[42,43]) and the cleavage sequence (0.8 nm). That is, the substrate extension without a P_7 spacer is smaller than the M^{pro} size, thus giving rise to steric effects.[41,44]

Peptide Ligand for Colorimetric (CM) Test. We next designed an all-peptide-based ligand (*i.e.*, CM-P_7) and coated it on AuNPs for colorimetric sensing of M^{pro}. Specifically, the CM-P_7 peptide was synthesized to encompass four functional domains (Figure 1c): (*i*) four Asp (D) residues for promoting colloidal stability and two Arg (R) residues for Coulombic interactions, (*ii*) an M^{pro} recognition site, (*iii*) a polyPro spacer, and (*iv*) a Cys anchor. The M^{pro} cleavage was confirmed by ESI-MS (Figure S1). Of note, this modular design can be reconfigured for other proteases by simply changing the enzyme recognition site. We hypothesized that the inclusion of a polyPro scaffold flanked by oppositely charged domains (*i.e.*, zwitterionic backbone, net charge = −2) in the peptide would promote enzyme accessibility and NP stabilization *via* an electrostatic double layer repulsion, respectively. After enzymatic cleavage, the positively charged peptide segment would bring the surface potential to neutrality and simultaneously induce plasmonic coupling with color changes.

Tight control of CM-P_7 fraction on the nanosurfaces was then realized by incorporating a backfiller ligand (*i.e.*, black squiggly line in Figure 1b). For this, we synthesized and compared three non-M^{pro} substrates to passivate gold surfaces: BF-D_1, BF-D_2, and BF-D_4, which contained 1, 2, and 4 Asp residues, respectively (Table S1).[49,55] Ligation with these backfillers had two important implications: (*i*) improving the colloidal stability and (*ii*) controlling the density of the M^{pro} substrate. Figure 3a,b shows the trend of hydrodynamic size (D_H) and zeta potential (ζ) of citrate–AuNPs incubated with the above backfillers at increasing concentrations (0–300 μM). AuNPs mixed with the BF-D_1 peptide (>5 μM) showed a rapid raising ζ from −30 to −5 mV, commensurate with particle aggregation manifesting in growing D_H. In comparison, no sizable changes were measured for AuNPs ligated with BF-D_2 and BF-D_4 regardless of the applied concentration. This indicates that the thiolated backfillers tethered with two or more Asp residues can compensate charge loss after substituting native citrate anions. BF-D_4 has a high charge valence, but it did not dramatically lower the surface potential even at high concentrations; the exact reason is unclear. We thus choose BF-D_2 as the backfiller for the next experiments. In practice, direct ligation of AuNPs with a mixture of BF-D_2 and

https://doi.org/10.1021/acs.nanolett.2c03052
Nano Lett. 2022, 22, 8932–8940

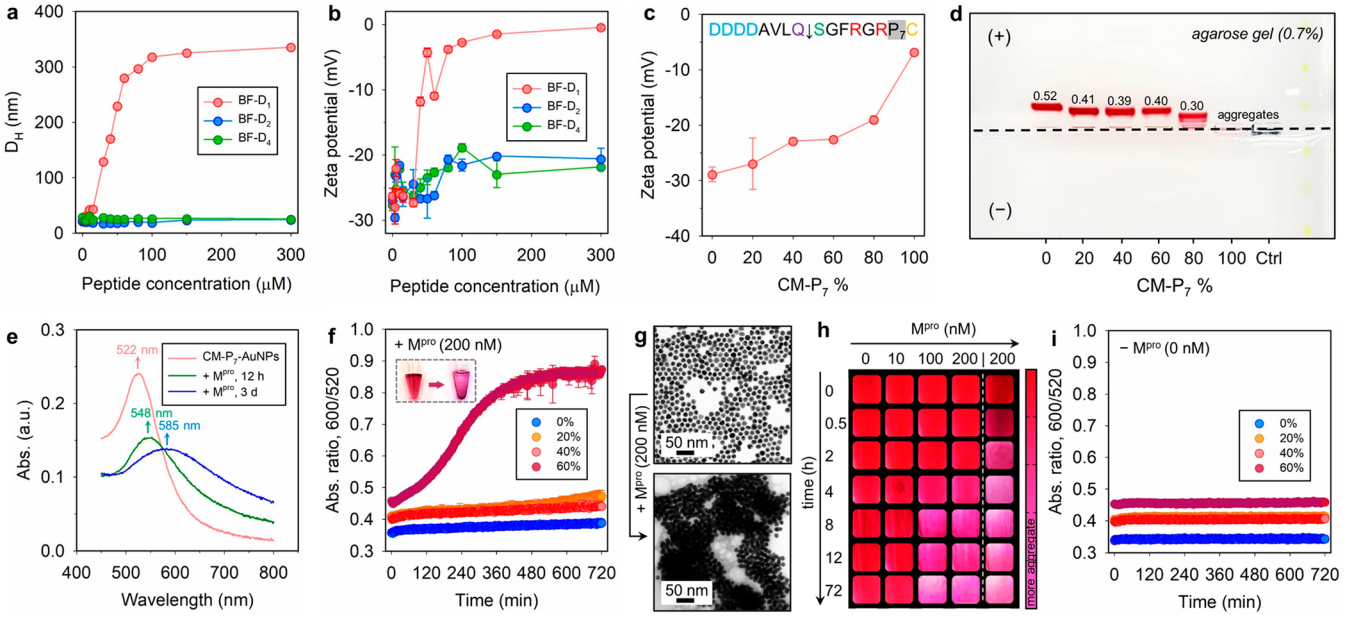

Figure 3. Activation of the colorimetric sensor by M^{pro}. Hydrodynamic size (a) and zeta potential (b) of citrate−AuNPs mixed with three sets of backfiller peptide (*i.e.*, BF-D_1, BF-D_2, and BF-D_4) at varying concentrations from 0 to 300 μM. Incubation time = 30 min. Zeta potential (c) and agarose gel (d) of AuNPs ligated with 0−100% CM-P_7. This peptide is combined with the BF-D_2 backfiller. AuNPs were unstable when CM-P_7 exceeds 80% (or $\zeta \geq -20$ mV) and the control band used citrate−AuNPs. The mobility shift is shown on the top of each band in cm. (e) Absorption of 60% CM-P_7−AuNPs (2.8 nM, 80 μL) incubated with M^{pro} (200 nM) at 0 min, 12 h, and 3 d. Red shifts of the SPR band were observed at 548 and 585 nm depending on incubation time. (f) Time progression of ratiometric absorbance (Abs_{600}/Abs_{520}) at 0−60% CM-P_7−AuNPs (2.8 nM, 80 μL) incubated with M^{pro} (200 nM). Phosphate buffer (10 mM, pH 8.0) was used, and the time interval is 2 min for 12 h. Error bar = standard deviation (duplicates). The inset shows the reaction color before and after proteolysis. (g) TEM images of the monodispersed 60% CM-P_7−AuNPs (top) and gold aggregates after proteolysis (bottom) by M^{pro}. (h) The M^{pro} concentration- and time-dependent color evolution of 60% CM-P_7−AuNPs (2.8 nM, 80 μL). *Remark:* the last column is collected from a mixture of 60% CM-P_7−AuNPs and citrate−AuNPs at a 1:1 equivalence. These are cropped images with a color bar where pink/purple represents particle flocculation. (i) Control tracks the time-dependent ratiometric absorbance of 0−60% CM-P_7−AuNPs (2.8 nM, 80 μL) without M^{pro}.

CM-P_7 ligands may cause irreversible aggregation. We thus optimized the immobilization strategy by first introducing BF-D_2 backfiller to AuNP dispersion (*i.e.*, 1 min incubation at 130,000 molar excess) followed by swift CM-P_7 addition; this provided a stable ligand exchange presumably due to the strong electrostatic repulsion rendered by backfillers.[55] Removal of these free ligands after exchange reaction was implemented using the same size exclusion chromatography as above (Figure 2b).[45,50] The peptide−AuNP conjugates were characterized using UV−vis spectroscopy, TEM, agarose gel (see below), and FT-IR[56] (Figure S5).

Figure 3c indicates the ζ of AuNPs immobilized with CM-P_7 and BF-D_2 peptide at varying molar ratios. A slight change from −30 to −20 mV was measured for AuNPs grafted with 0−60% CM-P_7, while a dramatic increase from −20 to near −5 mV occurred for 80% or more CM-P_7−AuNPs. The increase in surface potential was attributed to the high fraction of CM-P_7 carrying positively charged guanidine from Arg residues. Agarose gel analysis confirmed the same trend (Figure 3d): The mobility shift to the anode reduced as one increased the concentration of CM-P_7 on AuNPs. Notably, the bands of AuNPs with CM-P_7 exceeding 80% began to smear or aggregate, thus suggesting that a minimum amount of BF-D_2 backfiller was desired for good colloidal stability. A control band used pristine citrate−AuNPs and showed instant aggregation in the running buffer.

Protease Detection. M^{pro} regulates viral replication and transcription and is therefore an attractive diagnostic and therapeutic target for SARS-CoV-2.[41] Figure 3e shows an immediate difference between the absorption spectra of 60% CM-P_7−AuNPs (2.8 nM) with/without M^{pro} (200 nM). This condition yielded substrate and enzyme at a molar ratio of 10:1, using a total number of 1,200 ligands per NP estimated from the above NSET model. Clearly, enzymatic unveiling of 60% CM-P_7−AuNPs led to a pronounced decrease in the SPR band (*i.e.*, 522 nm) commensurate with a noticeable red shift to 548 nm at 12 h. A continuous monitoring of enzyme assays for 3 d resulted in a maximized aggregation with a broad band at 585 nm. Despite these two new bands after proteolysis, we still applied the ratiometric signal, Abs_{600}/Abs_{520}, for aggregation quantification due to the maximized signal difference (Figure S6).

Figure 3f shows the time-dependent ratiometric kinetics of 0 to 60% CM-P_7−AuNPs incubated with M^{pro} (200 nM). Only 60% CM-P_7−AuNPs had activated signals in 12 h proteolytic assay, while the other NP conjugates remained colloidally stable. TEM confirmed that the monodispersed AuNPs (before proteolysis) agglomerated significantly in the presence of M^{pro} (Figure 3g). This plasmonic coupling led to protease concentration- and time-dependent color changes from red to pink/purple (Figure 3h). A typical blue colored aggregation, however, was not observed due to trade-off of the polyPro scaffold at improving enzyme accessibility while restricting close proximity of neighbor metallic cores.[7,60,61] It is not unusual that assay time at hour scale was needed to maximize color changes due to (*i*) a low k_{cat}/K_M[52] and (*ii*) irregular enzymatic kinetic at cumbersome bio-NP interfaces.[62,63] Notably, ESI-MS measured the NP supernatant after

https://doi.org/10.1021/acs.nanolett.2c03052
Nano Lett. 2022, 22, 8932−8940

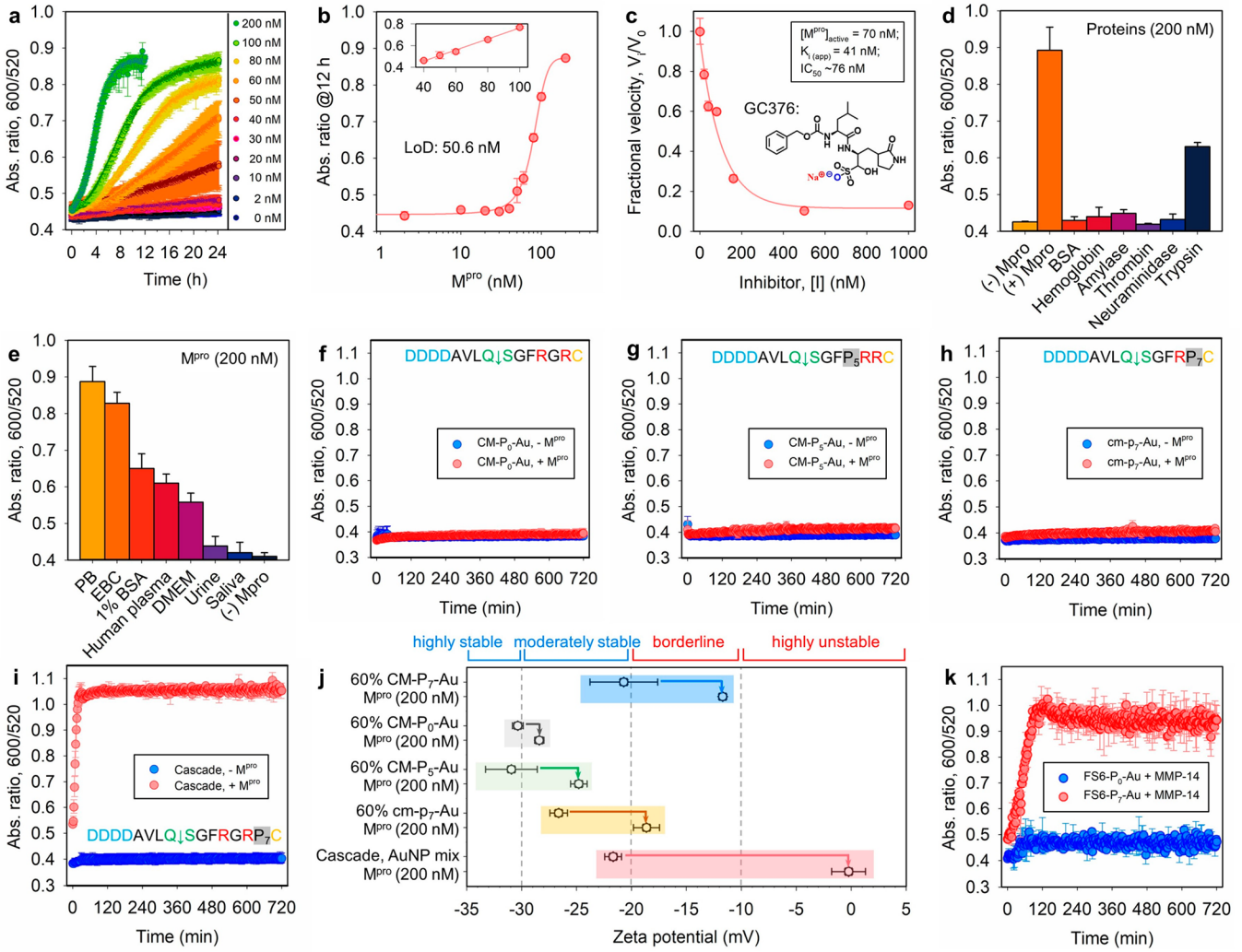

Figure 4. Sensitivity, specificity, and mechanistic study. (a) Time progression of the abs. ratio in enzyme assays, where 60% CM-P_7–AuNPs (2.8 nM, 80 μL) were incubated with increasing concentrations of M^{pro} (0–200 nM). Data were read every 2 min for 24 h. The curve using 200 nM M^{pro} is reproduced from Figure 3f. (b) The abs. ratio as a function of M^{pro} concentration was extracted from panel (a) at 12 h. The LoD is 50.6 nM in PB buffer. The inset shows the linear region used for LoD calculation. Error bar = standard deviation (duplicates). (c) Inhibition curve collected by titrating M^{pro} (100 nM) with varying amounts of GC376.[57] Error bar = standard deviation (triplicates). The inset shows the chemical structure of GC376 inhibitor. (d) Sensor performance interfered by other proteins (200 nM), including bovine serum albumin (BSA), hemoglobin, α-amylase (50 U/mL[58]), thrombin, influenza neuraminidase (5 U/mL[59]), and trypsin. Samples with and without M^{pro} were the controls. Error bar = standard deviation (triplicates). (e) Sensor performance in other biological media. Negative control used the sample without M^{pro}. Error bar = standard deviation (triplicates). Time progression of ratiometric absorbance, where CM-P_0–AuNPs (f), CM-P_5–AuNPs (g), cm-p_7–AuNPs (h), and a mixture of CM-P_7–AuNPs and citrate–AuNPs at a 1:1 equivalence (i) were incubated with/without M^{pro} (200 nM). The amount of AuNPs used was 2.8 nM, 80 μL, and the surfaces install 60% of target peptide. The peptide sequence is listed in each panel, and the cleavage site is marked with ↓. Error bar = standard deviation (duplicates). (j) Zeta potential of AuNPs after 12 h proteolysis showed a more-or-less increase when coated with 60% of CM-P_7, CM-P_0, CM-P_5, or cm-p_7 or in a cascade reaction. (k) Time progression of the abs. ratio in another protease assay, where 20% FS6-P_0–AuNPs and FS6-P_7–AuNPs (2.8 nM, 80 μL) were incubated with MMP-14 (30 nM).

proteolysis with the liberated Asp-rich fragment, D_4AVLQ (Figure S 1s). In contrast, negative control monitored the CM-P_7–AuNPs without M^{pro} and showed no color change (Figure 3i).

To study the limit of detection (LoD) for M^{pro} using the colorimetric sensor, enzyme assay was performed by incubating a fixed amount of 60% CM-P_7–AuNP conjugates (2.8 nM, 80 μL) with 0–200 nM of M^{pro} in phosphate buffer (10 mM, pH 8.0). In Figure 4a, the aggregation kinetics indicated that a higher amount of M^{pro} resulted in more particle aggregation and faster color change and *vice versa*. We set 12 h as the readout time, and Figure 4b plots the Abs_{600}/Abs_{520} ratio as a function of M^{pro} concentration. Thus, the LoD was calculated using a reported method and was 50.6 nM.[64] Despite this value being 2–5-fold higher than those of stepwise colorimetric sensors, it is similar to other one-step probes due to its unique configuration where all biochemical events took place *in situ*.[10,16,19,65]

Specificity Tests. The GC376 inhibitor was used to evaluate the enzymatic role of M^{pro} in colorimetric assays. M^{pro} (100 nM) was incubated with GC376 at varying molar ratios (*i.e.*, [I]/[E] = 0–10) for 10 min prior to mixing with the 60% CM-P_7–AuNP conjugates. Examination of the absorbance ratio at 12 h yields a typical inhibitor titration curve (Figure 4c). The Henderson equation (eq S18, Figure S8) estimated the active M^{pro} concentration to be 70 nM and the potency of

https://doi.org/10.1021/acs.nanolett.2c03052
Nano Lett. 2022, 22, 8932–8940

GC376 inhibitor to be $K_{i(app)}$ = 41 nM and IC_{50} = 76 nM.[66] These values at nanomolar range agree well with our previous work.[16]

The specificity of our system was further evaluated toward other proteins such as bovine serum albumin (BSA), hemoglobin, α-amylase, thrombin, influenza neuraminidase, and trypsin. In Figure 4d, no particle aggregation was detected in the presence of BSA, hemoglobin, and other enzymes. Trypsin did produce a false positive signal, albeit at a low level (~40%). ESI-MS on the supernatant of trypsin assay indicated that the CM-P_7 substrate was recognized by trypsin at the C-terminal of Arg at the P4′ site, thus liberating the Asp-rich segment and leading to AuNP aggregation (Figure S1t).

Matrix Effect. We evaluated matrix effects by first spiking M^{pro} in 10 μL of PB (10 mM, pH 8.0), exhaled breath condensate (EBC), BSA solution (1%), human plasma, DMEM cell culture media, urine, or human pooled saliva. Subsequently, the 60% CM-P_7−AuNP dispersion (2.8 nM, 80 μL) was added to reach a 200 nM protease concentration, and the abs. ratio at 12 h was recorded (Figure 4e). The AuNP conjugates worked best in buffer and EBC. BSA solution (1%), human plasma, and cell growth media impeded the aggregation kinetics presumably because negatively charged proteins scavenge the exposed positive charges on nanosurfaces. Urine and pooled human saliva, however, completely quenched the aggregation reactions. This has been reported in other literature[16,17] and is likely attributed to α-2-globulin (*i.e.*, a broad-spectrum protease inhibitor[67]) binding foreign proteins.

Mechanistic Studies. We next studied how subtle changes in peptide structure can significantly impact the NP interacting with biomolecules. This provides useful insights to customize substrates for one-step enzyme sensors with improved sensitivity. (*i*) *Role of polyPro*. We synthesized a CM-P_0 peptide (D_4AVLQ↓SGFRGRC)—an analogue of CM-P_7 but without a polyPro linker; see Figure 1c. In this scenario, 60% CM-P_0−AuNPs yielded no aggregation regardless of the M^{pro} presence (Figure 4f), thus stressing the critical role of spacer in promoting interfacial proteolysis. (*ii*) *Role of Arg/Asp*. The CM-P_5 peptide (D_4AVLQ↓SGF$\underline{P_5}$RRC) was then made by position-swapping the polyPro and Arg domains. This was intended to shorten the interparticle distance for better plasmonic coupling as in previous reports underlying charge-complementary interactions between guanidine and carboxylate groups.[16,18,24] Instead, no aggregation happened for M^{pro}-treated 60% CM-P_5−AuNPs (Figure 4g); this is presumably due to shielded Arg residues by prevalent polyPro at the exterior.[18] Similarly, there was no detectable aggregation regardless of M^{pro} in AuNPs capped with a cm-p7 peptide (D_3AVLQ↓SGFR$\underline{P_7}$C), where only one Arg was added (Figure 4h). This agrees with the notion that a threshold amount of Arg residue was required for charge cancellation and NP destabilization, as suggested in Figure 3f. However, ligand exchange of bare AuNPs with triple-Arg-containing peptide (D_5AVLQ↓SGFRGRR$\underline{P_7}$C, Figure S1r) could not yield conjugates of high quality because of rapid aggregation upon mixing. (*iii*) *Role of NP stability*. Furthermore, we designed a cascade AuNP dispersion consisting of a mixture of 60% CM-P_7−AuNPs and citrate−AuNPs at 1:1 equivalence, which remarkably boosted the M^{pro} response within an hour (Figure 4i). This increase in kinetics is due to citrate−AuNPs being extremely sensitive to minor changes in surface potential, thus causing a fast cascade aggregation at a high-cross-linking degree when exposed to low amounts of M^{pro}-processed 60% CM-P_7−AuNPs. Of note, the protease itself does not affect the dispersity of citrate−AuNPs (Figure S9).

The NP flocculation induced by electrostatic attraction was further corroborated with zeta potential measurement. Figure 4j shows surface potential of the above peptide−AuNPs before and after M^{pro} incubation for 12 h. The literature classifies NP dispersions with ζ-values of ±0−10 mV, ±10−20 mV, ±20−30 mV, and >±30 mV as highly unstable, borderline (un)stable, moderately stable, and highly stable, respectively, assuming that steric interactions scarcely contribute to current colloidal stability.[68] All the AuNP samples showed a rise on their ζ-value depending on the exact peptide architecture on nanosurfaces. For example, 60% CM-P_7−AuNPs and the cascade AuNP mixture had sizable ζ changes from near −22 mV to −11 mV and −2 mV, respectively. This manifested in colloid destabilization and color changes, which were particularly dramatic for the cascade dispersions. In comparison, both 60% CM-P_5−AuNPs and cm-p_7−AuNPs showed some loss of negative charges due to surface proteolysis liberating the Asp-stretching. However, their final ζ-values were still ±20−30 mV, and thus no NP aggregation. In contrast, the 60% CM-P_0−AuNPs showed essentially no ζ change due to a lack of surface proteolysis.

To this end, we also demonstrated that our modular peptide design can detect other proteases by tuning the specific cleavage site. Figure 4k shows that AuNPs conjugated with the FS6-P_7 peptide equipped with a P_7 linker responded the matrix metalloproteinase-14 (MMP-14[57,69]) and *vice versa*; see sequence in Table S1 and Figure S2. Also, despite that trypsin turned on the CM-P_7−AuNPs (Figure 4d), this did not occur to the CM-P_0−AuNPs (Figure S9).

In conclusion, we investigated how a spacer impacts the proteolytic activation of responsive nanosensors based on NSET or plasmonic coupling transduction mechanism. We designed a modular all-peptide-based ligand (CM-P_7) that incorporated a polyPro scaffold and zwitterionic backbone to promote enzyme accessibility and NP stabilization. We then coated this peptidic ligand onto 13 nm AuNPs and validated the conjugates for colorimetric protease sensing. The results showed that enzymatic unveiling of 60% CM-P_7−AuNPs by M^{pro} was successful, which induced color changes *via* electrostatic attraction. By quantifying color change with a measurable abs. ratio, we determined a LoD of 50.6 nM. Overall, this peptidic ligand allows for *in situ* occurrence of interfacial proteolysis and plasmonic coupling. The preparation does not require complex bioconjugations and postreaction evaluations and hence offers a simple and promising route for sensing other proteases.

■ ASSOCIATED CONTENT

Supporting Information

The Supporting Information is available free of charge at https://pubs.acs.org/doi/10.1021/acs.nanolett.2c03052.

Materials, instrumentation and characterization, peptide synthesis, AuNP synthesis, dye conjugation, ligand exchange, gel electrophoresis, NEST/FRET analysis, enzyme kinetics, inhibition/matrixes test, and MMP-14/trypsin detection; table of peptide library; figures of mass spectroscopy, NSET parameters, specificity constant and FRET analysis, FT-IR and absorption spectra, absorbance ratios, and TEM images (PDF)

https://doi.org/10.1021/acs.nanolett.2c03052
Nano Lett. 2022, 22, 8932−8940

AUTHOR INFORMATION

Corresponding Author

Jesse V. Jokerst − *Department of NanoEngineering, Materials Science and Engineering Program, and Department of Radiology, University of California, San Diego, La Jolla, California 92093, United States;* orcid.org/0000-0003-2829-6408; Email: jjokerst@ucsd.edu

Authors

Zhicheng Jin − *Department of NanoEngineering, University of California, San Diego, La Jolla, California 92093, United States;* orcid.org/0000-0001-6072-7533

Chuxuan Ling − *Department of NanoEngineering, University of California, San Diego, La Jolla, California 92093, United States*

Yi Li − *Department of NanoEngineering, University of California, San Diego, La Jolla, California 92093, United States*

Jiajing Zhou − *Department of NanoEngineering, University of California, San Diego, La Jolla, California 92093, United States;* orcid.org/0000-0001-5203-4737

Ke Li − *Institute of Materials Research and Engineering, Agency for Science, Technology and Research, Singapore 138634*

Wonjun Yim − *Materials Science and Engineering Program, University of California, San Diego, La Jolla, California 92093, United States;* orcid.org/0000-0002-0242-7898

Justin Yeung − *Department of Bioengineering, University of California San Diego, La Jolla, California 92093, United States*

Yu-Ci Chang − *Materials Science and Engineering Program, University of California, San Diego, La Jolla, California 92093, United States;* orcid.org/0000-0001-6997-9884

Tengyu He − *Materials Science and Engineering Program, University of California, San Diego, La Jolla, California 92093, United States;* orcid.org/0000-0002-6767-4849

Yong Cheng − *Department of NanoEngineering, University of California, San Diego, La Jolla, California 92093, United States*

Pavla Fajtová − *Skaggs School of Pharmacy and Pharmaceutical Sciences, University of California, San Diego, La Jolla, California 92093, United States*

Maurice Retout − *Department of NanoEngineering, University of California, San Diego, La Jolla, California 92093, United States*

Anthony J O'Donoghue − *Skaggs School of Pharmacy and Pharmaceutical Sciences, University of California, San Diego, La Jolla, California 92093, United States*

Complete contact information is available at: https://pubs.acs.org/10.1021/acs.nanolett.2c03052

Notes

The authors declare no competing financial interest.

ACKNOWLEDGMENTS

The authors thank internal fundings from the UC Office of the President (R00RG2515) and the National Institutes of Health (R01 DE031114; R21 AG065776-S1; R21 AI157957) for financial support. This work was also supported by National Science Foundation (DMR-2011924) via equipment in the UC San Diego Materials Research Science and Engineering Center (UCSD MRSEC). M.R. acknowledges the Wallonie-Bruxelles International (WBI) of the Fédération Wallonie-Bruxelles for financial support. The authors also thank Prof. Qing-Xiang Sang and Prof. Hedi Mattoussi (Florida State University, USA) for kindly providing the matrix metalloproteinase-14 as a gift. The electron microscopy work was performed in part at the San Diego Nanotechnology Infrastructure (SDNI) of University of California San Diego, a member of the National Nanotechnology Coordinated Infrastructure (NNCI), which is supported by the National Science Foundation (Grant ECCS-1542148).

REFERENCES

(1) Ye, D.; Shuhendler, A. J.; Cui, L.; Tong, L.; Tee, S. S.; Tikhomirov, G.; Felsher, D. W.; Rao, J. Bioorthogonal cyclization-mediated in situ self-assembly of small-molecule probes for imaging caspase activity in vivo. *Nat. Chem.* **2014**, *6*, 519−526.

(2) Sanman, L. E.; Bogyo, M. Activity-based profiling of proteases. *Annu. Rev. Biochem.* **2014**, *83*, 249−73.

(3) Boles, M. A.; Engel, M.; Talapin, D. V. Self-Assembly of Colloidal Nanocrystals: From Intricate Structures to Functional Materials. *Chem. Rev.* **2016**, *116*, 11220−11289.

(4) Grzelczak, M.; Liz-Marzán, L. M.; Klajn, R. Stimuli-responsive self-assembly of nanoparticles. *Chem. Soc. Rev.* **2019**, *48*, 1342−1361.

(5) Levin, A.; Hakala, T. A.; Schnaider, L.; Bernardes, G. J. L.; Gazit, E.; Knowles, T. P. J. Biomimetic peptide self-assembly for functional materials. *Nat. Rev. Chem.* **2020**, *4*, 615−634.

(6) Sheehan, F.; Sementa, D.; Jain, A.; Kumar, M.; Tayarani-Najjaran, M.; Kroiss, D.; Ulijn, R. V. Peptide-Based Supramolecular Systems Chemistry. *Chem. Rev.* **2021**, *121*, 13869−13914.

(7) Ghosh, S. K.; Pal, T. Interparticle Coupling Effect on the Surface Plasmon Resonance of Gold Nanoparticles: From Theory to Applications. *Chem. Rev.* **2007**, *107*, 4797−4862.

(8) Liu, X.; Zhang, Q.; Knoll, W.; Liedberg, B.; Wang, Y. Rational design of functional peptide−gold hybrid nanomaterials for molecular interactions. *Adv. Mater.* **2020**, *32*, 2000866.

(9) Zhou, J.; Creyer, M. N.; Chen, A.; Yim, W.; Lafleur, R. P. M.; He, T.; Lin, Z.; Xu, M.; Abbasi, P.; Wu, J.; Pascal, T. A.; Caruso, F.; Jokerst, J. V. Stereoselective Growth of Small Molecule Patches on Nanoparticles. *J. Am. Chem. Soc.* **2021**, *143*, 12138−12144.

(10) Jin, Z.; Yeung, J.; Zhou, J.; Cheng, Y.; Li, Y.; Mantri, Y.; He, T.; Yim, W.; Xu, M.; Wu, Z.; Fajtova, P.; Creyer, M. N.; Moore, C.; Fu, L.; Penny, W. F.; O'Donoghue, A. J.; Jokerst, J. V. Peptidic Sulfhydryl for Interfacing Nanocrystals and Subsequent Sensing of SARS-CoV-2 Protease. *Chem. Mater.* **2022**, *34*, 1259−1268.

(11) Liu, L.; Deng, D.; Wang, Y.; Song, K.; Shang, Z.; Wang, Q.; Xia, N.; Zhang, B. A colorimetric strategy for assay of protease activity based on gold nanoparticle growth controlled by ascorbic acid and Cu(II)-coordinated peptide. *Sens. Actuators B Chem.* **2018**, *266*, 246−254.

(12) Rossner, C.; Tang, Q.; Glatter, O.; Müller, M.; Vana, P. Uniform Distance Scaling Behavior of Planet−Satellite Nanostructures Made by Star Polymers. *Langmuir* **2017**, *33*, 2017−2026.

(13) Bera, S.; Mondal, S.; Xue, B.; Shimon, L. J. W.; Cao, Y.; Gazit, E. Rigid helical-like assemblies from a self-aggregating tripeptide. *Nat. Mater.* **2019**, *18*, 503−509.

(14) Álvarez, Z.; Kolberg-Edelbrock, A. N.; Sasselli, I. R.; Ortega, J. A.; Qiu, R.; Syrgiannis, Z.; Mirau, P. A.; Chen, F.; Chin, S. M.; Weigand, S.; Kiskinis, E.; Stupp, S. I. Bioactive scaffolds with enhanced supramolecular motion promote recovery from spinal cord injury. *Science* **2021**, *374*, 848−856.

(15) Bian, T.; Gardin, A.; Gemen, J.; Houben, L.; Perego, C.; Lee, B.; Elad, N.; Chu, Z.; Pavan, G. M.; Klajn, R. Electrostatic co-assembly of nanoparticles with oppositely charged small molecules into static and dynamic superstructures. *Nat. Chem.* **2021**, *13*, 940−949.

(16) Jin, Z.; Mantri, Y.; Retout, M.; Cheng, Y.; Zhou, J.; Jorns, A.; Fajtova, P.; Yim, W.; Moore, C.; Xu, M.; Creyer, M. N.; Borum, R. M.; Zhou, J.; Wu, Z.; He, T.; Penny, W. F.; O'Donoghue, A. J.;

Jokerst, J. V. A Charge-Switchable Zwitterionic Peptide for Rapid Detection of SARS-CoV-2 Main Protease. *Angew. Chem., Int. Ed.* **2022**, *61*, e202112995.
(17) Retout, M.; Mantri, Y.; Jin, Z.; Zhou, J.; Noël, G.; Donovan, B.; Yim, W.; Jokerst, J. V. Peptide-Induced Fractal Assembly of Silver Nanoparticles for Visual Detection of Disease Biomarkers. *ACS Nano* **2022**, *16*, 6165−6175.
(18) Huang, R. H.; Nayeem, N.; He, Y.; Morales, J.; Graham, D.; Klajn, R.; Contel, M.; O'Brien, S.; Ulijn, R. V. Self-Complementary Zwitterionic Peptides Direct Nanoparticle Assembly and Enable Enzymatic Selection of Endocytic Pathways. *Adv. Mater.* **2022**, *34*, 2104962.
(19) Feng, Y.; Liu, G.; La, M.; Liu, L. Colorimetric and Electrochemical Methods for the Detection of SARS-CoV-2 Main Protease by Peptide-Triggered Assembly of Gold Nanoparticles. *Molecules* **2022**, *27*, 615.
(20) Ruan, S.; Xiao, W.; Hu, C.; Zhang, H.; Rao, J.; Wang, S.; Wang, X.; He, Q.; Gao, H. Ligand-Mediated and Enzyme-Directed Precise Targeting and Retention for the Enhanced Treatment of Glioblastoma. *ACS Appl. Mater. Interfaces* **2017**, *9*, 20348−20360.
(21) Pelaz, B.; Jaber, S.; de Aberasturi, D. J.; Wulf, V.; Aida, T.; de la Fuente, J. M.; Feldmann, J.; Gaub, H. E.; Josephson, L.; Kagan, C. R.; Kotov, N. A.; Liz-Marzán, L. M.; Mattoussi, H.; Mulvaney, P.; Murray, C. B.; Rogach, A. L.; Weiss, P. S.; Willner, I.; Parak, W. J. The State of Nanoparticle-Based Nanoscience and Biotechnology: Progress, Promises, and Challenges. *ACS Nano* **2012**, *6*, 8468−8483.
(22) Fleming, A.; Cursi, L.; Behan, J. A.; Yan, Y.; Xie, Z.; Adumeau, L.; Dawson, K. A. Designing Functional Bionanoconstructs for Effective In Vivo Targeting. *Bioconjugate Chem.* **2022**, *33*, 429−443.
(23) Mirkin, C. A.; Letsinger, R. L.; Mucic, R. C.; Storhoff, J. J. A DNA-based method for rationally assembling nanoparticles into macroscopic materials. *Nature* **1996**, *382*, 607−609.
(24) Guo, L.; Xu, Y.; Ferhan, A. R.; Chen, G.; Kim, D.-H. Oriented Gold Nanoparticle Aggregation for Colorimetric Sensors with Surprisingly High Analytical Figures of Merit. *J. Am. Chem. Soc.* **2013**, *135*, 12338−12345.
(25) Claridge, S. A.; Mastroianni, A. J.; Au, Y. B.; Liang, H. W.; Micheel, C. M.; Fréchet, J. M. J.; Alivisatos, A. P. Enzymatic Ligation Creates Discrete Multinanoparticle Building Blocks for Self-Assembly. *J. Am. Chem. Soc.* **2008**, *130*, 9598−9605.
(26) Stevens, M. M.; Flynn, N. T.; Wang, C.; Tirrell, D. A.; Langer, R. Coiled-Coil Peptide-Based Assembly of Gold Nanoparticles. *Adv. Mater.* **2004**, *16*, 915−918.
(27) Heuer-Jungemann, A.; Feliu, N.; Bakaimi, I.; Hamaly, M.; Alkilany, A.; Chakraborty, I.; Masood, A.; Casula, M. F.; Kostopoulou, A.; Oh, E.; Susumu, K.; Stewart, M. H.; Medintz, I. L.; Stratakis, E.; Parak, W. J.; Kanaras, A. G. The Role of Ligands in the Chemical Synthesis and Applications of Inorganic Nanoparticles. *Chem. Rev.* **2019**, *119*, 4819−4880.
(28) González-Fernández, E.; Staderini, M.; Avlonitis, N.; Murray, A. F.; Mount, A. R.; Bradley, M. Effect of spacer length on the performance of peptide-based electrochemical biosensors for protease detection. *Sens. Actuators B Chem.* **2018**, *255*, 3040−3046.
(29) Moitra, P.; Alafeef, M.; Dighe, K.; Frieman, M. B.; Pan, D. Selective Naked-Eye Detection of SARS-CoV-2 Mediated by N Gene Targeted Antisense Oligonucleotide Capped Plasmonic Nanoparticles. *ACS Nano* **2020**, *14*, 7617−7627.
(30) Martić, S.; Labib, M.; Freeman, D.; Kraatz, H.-B. Probing the Role of the Linker in Ferrocene−ATP Conjugates: Monitoring Protein Kinase Catalyzed Phosphorylations Electrochemically. *Chem.—Eur. J.* **2011**, *17*, 6744−6752.
(31) De Fazio, A. F.; El-Sagheer, A. H.; Kahn, J. S.; Nandhakumar, I.; Burton, M. R.; Brown, T.; Muskens, O. L.; Gang, O.; Kanaras, A. G. Light-Induced Reversible DNA Ligation of Gold Nanoparticle Superlattices. *ACS Nano* **2019**, *13*, 5771−5777.
(32) Guarise, C.; Pasquato, L.; De Filippis, V.; Scrimin, P. Gold nanoparticles-based protease assay. *Proc. Natl. Acad. Sci. U.S.A.* **2006**, *103*, 3978−3982.
(33) Creyer, M. N.; Jin, Z.; Moore, C.; Yim, W.; Zhou, J.; Jokerst, J. V. Modulation of Gold Nanorod Growth via the Proteolysis of Dithiol Peptides for Enzymatic Biomarker Detection. *ACS Appl. Mater. Interfaces* **2021**, *13*, 45236−45243.
(34) Yang, K.; Liu, Y.; Wang, Y.; Ren, Q.; Guo, H.; Matson, J. B.; Chen, X.; Nie, Z. Enzyme-induced in vivo assembly of gold nanoparticles for imaging-guided synergistic chemo-photothermal therapy of tumor. *Biomaterials* **2019**, *223*, 119460.
(35) Jin, Z.; Kapur, A.; Wang, W.; Hernandez, J. D.; Thakur, M.; Mattoussi, H. The dual−function of lipoic acid groups as surface anchors and sulfhydryl reactive sites on polymer−stabilized QDs and Au nanocolloids. *J. Chem. Phys.* **2019**, *151*, 164703.
(36) Graham, B.; Bailey, T. L.; Healey, J. R. J.; Marcellini, M.; Deville, S.; Gibson, M. I. Polyproline as a Minimal Antifreeze Protein Mimic That Enhances the Cryopreservation of Cell Monolayers. *Angew. Chem., Int. Ed.* **2017**, *56*, 15941−15944.
(37) Hung, J. J.; Dear, B. J.; Dinin, A. K.; Borwankar, A. U.; Mehta, S. K.; Truskett, T. T.; Johnston, K. P. Improving Viscosity and Stability of a Highly Concentrated Monoclonal Antibody Solution with Concentrated Proline. *Pharm. Res.* **2018**, *35*, 133.
(38) Xia, N.; Huang, Y.; Cui, Z.; Liu, S.; Deng, D.; Liu, L.; Wang, J. Impedimetric biosensor for assay of caspase-3 activity and evaluation of cell apoptosis using self-assembled biotin-phenylalanine network as signal enhancer. *Sens. Actuators B Chem.* **2020**, *320*, 128436.
(39) Nowinski, A. K.; Sun, F.; White, A. D.; Keefe, A. J.; Jiang, S. Sequence, Structure, and Function of Peptide Self-Assembled Monolayers. *J. Am. Chem. Soc.* **2012**, *134*, 6000−6005.
(40) Egorova, E. A.; van Rijt, M. M. J.; Sommerdijk, N.; Gooris, G. S.; Bouwstra, J. A.; Boyle, A. L.; Kros, A. One Peptide for Them All: Gold Nanoparticles of Different Sizes Are Stabilized by a Common Peptide Amphiphile. *ACS Nano* **2020**, *14*, 5874−5886.
(41) Jin, Z.; Du, X.; Xu, Y.; Deng, Y.; Liu, M.; Zhao, Y.; Zhang, B.; Li, X.; Zhang, L.; Yang, H. Structure of Mpro from SARS-CoV-2 and discovery of its inhibitors. *Nature* **2020**, *582*, 289−293.
(42) Schuler, B.; Lipman, E. A.; Steinbach, P. J.; Kumke, M.; Eaton, W. A. Polyproline and the spectroscopic ruler; revisited with single-molecule fluorescence. *Proc. Natl. Acad. Sci. U.S.A.* **2005**, *102*, 2754−2759.
(43) Algar, W. R.; Malonoski, A.; Deschamps, J. R.; Blanco-Canosa, J. B.; Susumu, K.; Stewart, M. H.; Johnson, B. J.; Dawson, P. E.; Medintz, I. L. Proteolytic Activity at Quantum Dot-Conjugates: Kinetic Analysis Reveals Enhanced Enzyme Activity and Localized Interfacial "Hopping. *Nano Lett.* **2012**, *12*, 3793−3802.
(44) Erickson, H. P. Size and Shape of Protein Molecules at the Nanometer Level Determined by Sedimentation, Gel Filtration, and Electron Microscopy. *Biol. Proced. Online* **2009**, *11*, 32.
(45) Yang, M.; Moroz, P.; Jin, Z.; Budkina, D. S.; Sundrani, N.; Porotnikov, D.; Cassidy, J.; Sugiyama, Y.; Tarnovsky, A. N.; Mattoussi, H.; Zamkov, M. Delayed Photoluminescence in Metal-Conjugated Fluorophores. *J. Am. Chem. Soc.* **2019**, *141*, 11286−11297.
(46) Singh, M. P.; Strouse, G. F. Involvement of the LSPR Spectral Overlap for Energy Transfer between a Dye and Au Nanoparticle. *J. Am. Chem. Soc.* **2010**, *132*, 9383−9391.
(47) Turkevich, J.; Stevenson, P. C.; Hillier, J. A study of the nucleation and growth processes in the synthesis of colloidal gold. *Discuss. Faraday Soc.* **1951**, *11*, 55−75.
(48) Rawlings, N. D.; Waller, M.; Barrett, A. J.; Bateman, A. Peptidase specificity. 2014. *MEROPS database*. https://www.ebi.ac.uk/merops/cgi-bin/peptidase_specificity (accessed Apr 18, 2022).
(49) Susumu, K.; Mei, B. C.; Mattoussi, H. Multifunctional ligands based on dihydrolipoic acid and polyethylene glycol to promote biocompatibility of quantum dots. *Nat. Protocols* **2009**, *4*, 424−436.
(50) Linkov, P.; Samokhvalov, P.; Grokhovsky, S.; Laronze-Cochard, M.; Sapi, J.; Nabiev, I. Selection of the Optimal Chromatography Medium for Purification of Quantum Dots and Their Bioconjugates. *Chem. Mater.* **2020**, *32*, 9078−9089.

https://doi.org/10.1021/acs.nanolett.2c03052
Nano Lett. 2022, 22, 8932−8940

(51) Liu, X.; Atwater, M.; Wang, J.; Huo, Q. Extinction coefficient of gold nanoparticles with different sizes and different capping ligands. *Colloids Surf. B Biointerfaces* **2007**, *58*, 3−7.
(52) Zhang, L.; Lin, D.; Sun, X.; Curth, U.; Drosten, C.; Sauerhering, L.; Becker, S.; Rox, K.; Hilgenfeld, R. Crystal structure of SARS-CoV-2 main protease provides a basis for design of improved ketoamide inhibitors. *Science* **2020**, *368*, 409−412.
(53) Shan, Y. F.; Xu, G. J. Study on substrate specificity at subsites for severe acute respiratory syndrome coronavirus 3CL protease. *Acta. Biochim. Biophys. Sin.* **2005**, *37*, 807−13.
(54) Moroz, P.; Jin, Z.; Sugiyama, Y.; Lara, D. A.; Razgoniaeva, N.; Yang, M.; Kholmicheva, N.; Khon, D.; Mattoussi, H.; Zamkov, M. Competition of Charge and Energy Transfer Processes in Donor−Acceptor Fluorescence Pairs: Calibrating the Spectroscopic Ruler. *ACS Nano* **2018**, *12*, 5657−5665.
(55) Olmedo, I.; Araya, E.; Sanz, F.; Medina, E.; Arbiol, J.; Toledo, P.; Álvarez-Lueje, A.; Giralt, E.; Kogan, M. J. How Changes in the Sequence of the Peptide CLPFFD-NH2 Can Modify the Conjugation and Stability of Gold Nanoparticles and Their Affinity for β-Amyloid Fibrils. *Bioconjugate Chem.* **2008**, *19*, 1154−1163.
(56) Jin, Z.; Du, L.; Zhang, C.; Sugiyama, Y.; Wang, W.; Palui, G.; Wang, S.; Mattoussi, H. Modification of Poly(maleic anhydride)-Based Polymers with H2N−R Nucleophiles: Addition or Substitution Reaction? *Bioconjugate Chem.* **2019**, *30*, 871−880.
(57) Hurst, D. R.; Schwartz, M. A.; Ghaffari, M. A.; Jin, Y.; Tschesche, H.; Fields, G. B.; Sang, Q.-X. A. Catalytic- and ecto-domains of membrane type 1-matrix metalloproteinase have similar inhibition profiles but distinct endopeptidase activities. *Biochem. J.* **2004**, *377*, 775−779.
(58) Jin, Z.; Jorns, A.; Yim, W.; Wing, R.; Mantri, Y.; Zhou, J.; Zhou, J.; Wu, Z.; Moore, C.; Penny, W. F.; Jokerst, J. V. Mapping Aerosolized Saliva on Face Coverings for Biosensing Applications. *Anal. Chem.* **2021**, *93*, 11025−11032.
(59) Lin, X.; Liu, X.-Y.; Zhang, B.; Qin, A.-Q.; Hui, K.-M.; Shi, K.; Liu, Y.; Gabriel, D.; Li, X. J. A rapid influenza diagnostic test based on detection of viral neuraminidase activity. *Sci. Rep.* **2022**, *12*, 505.
(60) Zhong, Z.; Patskovskyy, S.; Bouvrette, P.; Luong, J. H. T.; Gedanken, A. The Surface Chemistry of Au Colloids and Their Interactions with Functional Amino Acids. *J. Phys. Chem. B* **2004**, *108*, 4046−4052.
(61) Su, K. H.; Wei, Q. H.; Zhang, X.; Mock, J. J.; Smith, D. R.; Schultz, S. Interparticle Coupling Effects on Plasmon Resonances of Nanogold Particles. *Nano Lett.* **2003**, *3*, 1087−1090.
(62) Algar, W. R.; Jeen, T.; Massey, M.; Peveler, W. J.; Asselin, J. Small Surface, Big Effects, and Big Challenges: Toward Understanding Enzymatic Activity at the Inorganic Nanoparticle−Substrate Interface. *Langmuir* **2019**, *35*, 7067−7091.
(63) Ma, J.; Hou, S.; Lu, D.; Zhang, B.; Xiong, Q.; Chan-Park, M. B.; Duan, H. Caging Cationic Polymer Brush-Coated Plasmonic Nanostructures for Traceable Selective Antimicrobial Activities. *Macromol. Rapid Commun.* **2022**, *43*, 2100812.
(64) Armbruster, D. A.; Pry, T. Limit of blank, limit of detection and limit of quantitation. *Clin. Biochem. Rev.* **2008**, *29* (1), S49−S52.
(65) Moore, C.; Borum, R. M.; Mantri, Y.; Xu, M.; Fajtová, P.; O'Donoghue, A. J.; Jokerst, J. V. Activatable Carbocyanine Dimers for Photoacoustic and Fluorescent Detection of Protease Activity. *ACS Sens.* **2021**, *6*, 2356−2365.
(66) Henderson, P. J. A linear equation that describes the steady-state kinetics of enzymes and subcellular particles interacting with tightly bound inhibitors. *Biochem. J.* **1972**, *127*, 321−333.
(67) Vandooren, J.; Itoh, Y. Alpha-2-Macroglobulin in Inflammation, Immunity and Infections. *Front. Immunol.* **2021**, DOI: 10.3389/fimmu.2021.803244.
(68) Bhattacharjee, S. DLS and zeta potential − What they are and what they are not? *J. Controlled Release* **2016**, *235*, 337−351.
(69) Neumann, U.; Kubota, H.; Frei, K.; Ganu, V.; Leppert, D. Characterization of Mca-Lys-Pro-Leu-Gly-Leu-Dpa-Ala-Arg-NH2, a fluorogenic substrate with increased specificity constants for collagenases and tumor necrosis factor converting enzyme. *Anal. Biochem.* **2004**, *328*, 166−173.

https://doi.org/10.1021/acs.nanolett.2c03052
Nano Lett. 2022, 22, 8932−8940